Desalination and Water Treatment
www.deswater.com

doi: 10.5004/dwt.2022.28746

270 (2022) 236–244
September

Preparation of nanoparticles-assembled Cu_2O microspheres by ultrasound-assisted polyol process and their adsorption performance

Yonggang Peng[a,*], Yongqiang Feng[a], Yongxin Tao[a], Huaixin Wan[b]

[a]*Jiangsu Key Laboratory of Advanced Catalytic Materials and Technology, School of Petrochemical Engineering, Changzhou University, Changzhou 213164, China, Tel. +86 051986330263; emails: pengyonggang@cczu.edu.cn (Y. Peng), 1402633038@qq.com (Y. Feng), taoyx@cczu.edu.cn (Y. Tao)*
[b]*Jiangsu Maige Sorbent Co., Ltd., Huai'an 211700, China, Tel. +86 051788281238; email: 940730799@qq.com (H. Wan)*

Received 24 March 2022; Accepted 23 July 2022

ABSTRACT

Cuprous oxide microspheres (Cu_2O SPs) assembled by nanoparticles were successfully prepared via a facile ultrasound-assisted polyol process using cupric acetate monohydrate as a precursor and diethylene glycol as both solvent and reducing agent, and characterized by X-ray diffraction, scanning electron microscopy, transmission electron microscopy and nitrogen adsorption–desorption. Results showed that the as-prepared product was cubic Cu_2O without any impurity and displayed microsphere morphologies with diameters of 250–300 nm, which were assembled by nanoparticles. The as-prepared Cu_2O SPs exhibited excellent adsorption capability for methyl orange (MO). Kinetics and isotherms studies showed that the adsorption process of MO onto Cu_2O SPs followed pseudo-second-order and Langmuir models. The maximum MO adsorption capability according to the Langmuir model under different concentrations ranging from 90 to 300 mg/L was estimated to be 885.0 mg/g. Moreover, Cu_2O SPs can be regenerated by photocatalytic degradation of adsorbed MO.

Keywords: Ultrasound; Adsorption; Cu_2O microspheres; Polyol process; Dye; Methyl orange

1. Introduction

In recent years, the arbitrary discharge of dye wastewater has become one of the most serious environmental issues because organic dyes are widely used in cosmetics, rubber, food, leather, printing and textile industries [1,2]. A small amount of dye wastewater discharged into the hydrosphere often affects the aesthetics of water bodies, decreases light penetration, hinders the photosynthesis of the aquatic plants and even induces toxicity to aquatic life [3,4]. Therefore, removing organic dyes from wastewater prior to discharge into hydrosphere is highly important for environmental protection and human's health.

Various methods have been explored to deal with dye wastewater, including advanced oxidation [5], adsorption [6], ion-exchange [7], membrane separation [8] and so on. Among these methods, adsorption is deemed as a promising approach due to simple operation, low cost and energy requirement [9]. Many adsorbents have been developed, such as silica microspheres [10], carbon-based materials [11], organoclays [12], magnetic nanoparticles [13–16], metal-organic frameworks [17], as well as organic polymers [18]. However, most of the aforementioned adsorbents still have some disadvantages (e.g., low adsorption capacity, complicated preparation process, or high cost) [19].

Recently, cuprous oxide (Cu_2O) has been paid much attention due to its low cost, low toxicity, abundant availability and easy accessibility [20], which has been widely used in gas sensors, lithium ion batteries, solar energy conversion, hydrogen evolution, and degradation of

* Corresponding author.

organic pollutants in wastewater [21]. It also has a potential application in adsorption of organic dyes from wastewater [22–23]. The polyol method is one of the common techniques for the preparation of Cu_2O. In this process, polyol not only acts as a solvent and reducing agent, but also acts as a stabilizer and capping agent, limiting particle growth and preventing their agglomeration [24]. However, the reaction often requires high temperature (160°C–190°C) for a long time (2–6 h) [25,26].

Ultrasonic irradiation can produce local hot spots with extremely high temperature and pressure even at room temperature in bulk [27], which provides a favorable environment for the formation of nanoparticles. Herein, Cu_2O microspheres (Cu_2O SPs) were prepared via ultrasound-assisted polyol process, and the adsorption performance of methyl orange (MO) onto Cu_2O SPs was investigated.

2. Experimental

2.1. Materials

Cupric acetate monohydrate ($Cu(CH_3COO)_2{\cdot}H_2O$), diethylene glycol (DEG), methyl orange ($C_{14}H_{14}N_3SO_3Na$, MO), congo red ($C_{32}H_{22}N_6Na_2O_6S_2$, CR), methylene blue ($C_{16}H_{18}ClN_3S$, MB) and rhodamine B ($C_{28}H_{31}ClN_2O_3$, RB) were purchased from Sinopharm Chemical Reagent Co., Ltd., (China). All the reagents were used as received without any further purification.

2.2. Preparation of Cu_2O SPs

Typically, $Cu(OOCCH_3)_2{\cdot}H_2O$ (1.0 g) was dissolved into 40 mL of diethylene glycol under mechanical stirring, and 1 mL deionized water was added to the above solution. Then the solution was further treated by an ultrasonic T-horn (Manufactured by Nanjing Xian'ou Instrument Co., Ltd., China) at 480 W of dissipated power for 30 min on 1 s pulse mode (1 s on mode and 1 s off mode). The titanium tip of the horn was located at the center of the solution and immersed 1 cm deep in it. During the ultrasonic process, the solution was placed in a cooling bath, keeping a constant temperature of 30°C. After that, the obtained product was centrifuged, washed several times with absolute alcohol and deionized water, and then dried under vacuum at 60°C overnight.

2.3. Characterization

The crystal structure of the product was determined by power X-ray diffraction at room temperature using a PANalytical X'Pert diffractometer with Cu K_α radiation (λ = 0.154 nm), running at 40 kV and 30 mA. The morphologies of the sample were characterized by a JEOL JEM-2100 transmission electron microscopy (TEM) with an acceleration voltage of 300 kV and a JEOL JSM-6380LV scanning electron microscopy (SEM) with an acceleration voltage of 10 kV. N_2 adsorption–desorption isotherm was carried out on a Micromeritics ASAP 2020 nitrogen adsorption apparatus (USA). The size distribution of Cu_2O SPs was determined by dynamic light scattering (DLS) method using ZEN3600 zetasizer (Malvern instruments, UK).

2.4. Adsorption experiments

All adsorption experiments were carried out using 15 mg Cu_2O SPs and 50 mL MO solution on a thermostatic oscillator at 30°C unless otherwise stated. In adsorption kinetics experiments, the concentrations of MO solutions were 100, 200, and 300 mg/L, respectively, and the pH value of solutions was about neutral. For adsorption isotherms experiments, MO concentrations ranged from 90 to 300 mg/L at neutral pH and 30°C. After the adsorption experiment, the mixtures were centrifuged and the dye concentration of the supernatant was measured using a UV-vis spectrophotometer at a maximum adsorption wavelength of 464 nm. The adsorption amount of MO per unit mass of Cu_2O SPs at any time was calculated by Eq. (1).

$$q_t = \frac{C_0 - C_t}{m} \times V \tag{1}$$

where q_t (mg/g) is the adsorption capacity of adsorbents at time t; C_0 (mg/L) and C_t (mg/L) are the concentrations of MO initially and at any time t, respectively; V (L) is the volume of MO solution; and m (g) is the mass of Cu_2O SPs.

3. Results and discussion

3.1. Characterization of Cu_2O SPs

Fig. 1 shows the typical X-ray diffraction (XRD) pattern of as-prepared Cu_2O SPs. The main peaks at 29.6°, 36.4°, 42.3°, 61.4°, 73.5° and 77.4° are correspond to the (110), (111), (200), (220), (311) and (222) crystalline planes of cubic Cu_2O (JCPDS78-2076) [28], respectively. No other impurities related to Cu, CuO or $Cu(OH)_2$ are detected, suggesting the as-prepared Cu_2O SPs have high purity.

The SEM and TEM images of Cu_2O SPs are shown in Fig. 2a–d. Fig. 2a and b distinctly indicate that the as-prepared sample is spherical-like with diameter in 250–300 nm. A few Cu_2O SPs agglomerate together and each Cu_2O microsphere is assembled by a lot of nanoparticles. Cu_2O SPs have rough surfaces and porous structures, and some of the Cu_2O SPs have small cavity as indicated by red arrows. The typical TEM images (Fig. 2c and d) further confirm that Cu_2O SPs are mainly composed of numerous primary nanoparticles and a large number of pores exist between nanoparticles, which is consistent with the SEM observation. Fig. 2e shows the size distribution of synthesized Cu_2O SPs determined by DLS technique. The average particle size of Cu_2O SPs was about 335.3 nm, which is close to the results of SEM and TEM analysis.

The N_2 adsorption–desorption isotherm and pore-size distribution of Cu_2O SPs are shown in Fig. 3 and its inset, respectively. The isotherm of Cu_2O SPs is classified as type IV with a type H_2 hysteresis loop at the relative pressure (P/P_0) range from 0.7 to 1.0, which is the typical characteristic of slit-like pores formed by nanoparticles [29,30]. The Brunauer–Emmett–Teller surface area and the pore volume of the Cu_2O SPs calculated from the adsorption–desorption isotherm are 23.3 m^2/g and 87.5 mm^3/g, respectively. The pore-size distribution curve of Cu_2O SPs shows a broad pore range from 3 to 60 nm (inset in Fig. 3).

In the process of preparing Cu_2O SPs by polyol method, water plays a critical role. As was reported by Yu et al. [31], no Cu_2O but metal copper nanoparticles were formed without adding water by traditional polyol process using cupric acetate monohydrate as precursor and diethylene glycol as solvent. According to the above fact, a possible formation mechanism of Cu_2O SPs was proposed as follows. Firstly, Cu^{2+} hydrolyzed to form $Cu(OH)_2$ [as Eq. (2)], and then $Cu(OH)_2$ was reduced by DEG under ultrasonic irradiation by Eq. (3). Because DEG could combine with Cu^{2+} through Cu–O covalent and/or Cu–OH coordination bonds [32], the growth of Cu_2O nanoparticles is limited. And the sizes of Cu_2O obtained using the polyol process by high temperature are about 10 nm [31]. In the ultrasonic process, high temperature is only formed locally in the bulk solution. Nanoparticles formed around the hot spots produced by ultrasonic irradiation were further assembled in the bulk solution to form Cu_2O SPs.

$$Cu(OOCCH_3)_2 + H_2O \rightarrow Cu(OH)_2 + 2CH_3COOH \quad (2)$$

$$2Cu(OH)_2 + HOCH_2CH_2OCH_2CH_2OH \xrightarrow{)))} Cu_2O + HOCH_2CH_2OCH_2CHO + 3H_2O \quad (3)$$

3.2. Adsorption experiments

Two cationic dyes (MB, RB) and two anionic dyes (MO, CR) were used to evaluate the adsorption performance of Cu_2O SPs. As shown in Fig. 4, the removal efficiency of MO and CR were 99.2% and 98.5%, respectively. However, the adsorption performance of Cu_2O SPs to cationic dyes was very poor, and the removal efficiency of MB and RB were 15.3% and 10.6%, respectively. The measured zeta potential of Cu_2O SPs was 3.36 mV. Strong electrostatic attraction between the positively charged surface of Cu_2O SPs and the negatively charged sulfonic acid group of MO and CR may be the main reason for the excellent adsorption performance of Cu_2O SPs for two anionic dyes [33]. In addition, the special pore structure of Cu_2O SPs is also favorable to the diffusion of anionic dyes into the material.

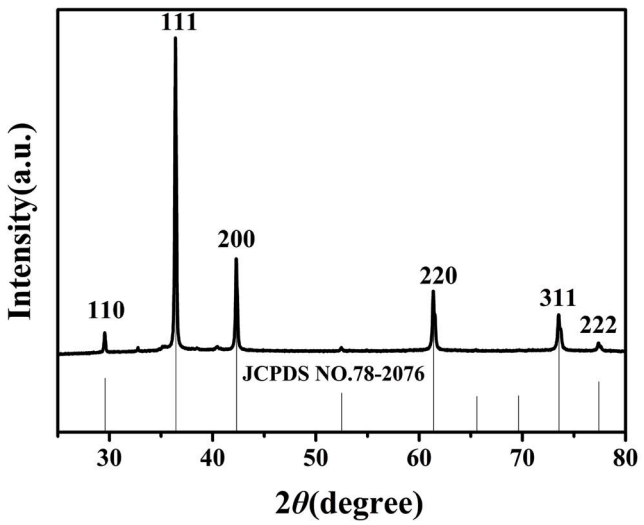

Fig. 1. XRD pattern of Cu_2O SPs.

3.2.1. Adsorption kinetics

The research on adsorption kinetics and isotherms is of vital importance to investigate the adsorption behaviors of Cu_2O SPs. As a representative anionic dye, MO was used to study the adsorption kinetics and isotherms of Cu_2O SPs. Fig. 5 shows the effect of contact times and initial dye concentrations on the adsorption capacity of MO onto Cu_2O SPs. The adsorption capacity displayed a sharp increase in the initial stage, followed by a gradual increase until the equilibrium stage was reached. The adsorption capacity increased with the increase of the initial MO concentration. The reason might be that MO was firstly adsorbed on the surface of Cu_2O SPs and then progressively diffused into the inside with the prolongation of adsorption time [34]. At the low initial concentration (100 mg/L), the adsorption equilibrium was soon reached. However, the time to reach adsorption equilibrium is more than 18 h at the high initial concentration (300 mg/L).

To further understand the adsorption process, the pseudo-first-order, pseudo-second-order diffusion models and intraparticle diffusion model were employed to analyze the adsorption kinetics. The linear equations of three common models are expressed as follows [35,36]:

$$\text{Pseudo-first-order model: } \ln(q_e - q_t) = \ln q_e - k_1 t \quad (4)$$

$$\text{Pseudo-second-order model: } \frac{t}{q_t} = \frac{1}{k_2 q_e^2} + \frac{t}{q_e} \quad (5)$$

$$\text{Intraparticle diffusion model: } q_t = k_i t^{0.5} + c_i \quad (6)$$

where q_e and q_t (mg/g) are the adsorption capacity at equilibrium and at time t, respectively. k_1 (h^{-1}) and k_2 (g/mg h) are rate constants for pseudo-first-order and pseudo-second-order models, respectively. k_i is the intraparticle diffusion rate constant (mg/g $h^{1/2}$) at stage i and c_i is a constant (mg/g).

The fitting curves of the pseudo-first-order and pseudo-second-order kinetics are exhibited in Fig. 6a and b. The parameters and correlation coefficients (R^2) are summarized in Table 1. For the pseudo-first-order model, the calculated $q_{e,cal}$ value significantly deviates from the experimental $q_{e,exp}$ and the correlation coefficient (R^2) is relatively low. In contrast, the calculated $q_{e,cal}$ value for the pseudo-second-order model is good agreement with the experimental $q_{e,exp}$, and the correlation coefficient (R^2) reaches 0.999, which indicates that the pseudo-second-order kinetic model is more appropriate for describing the adsorption process of MO onto the prepared Cu_2O SPs.

The intraparticle diffusion kinetics model was used to study the rate control steps of the adsorption process (Fig. 6c) and the corresponding parameters are summarized in Table 2. According to Fig. 6c, the slope of q_t to $t^{1/2}$ is not linear and deviates from the origin, which indicates three

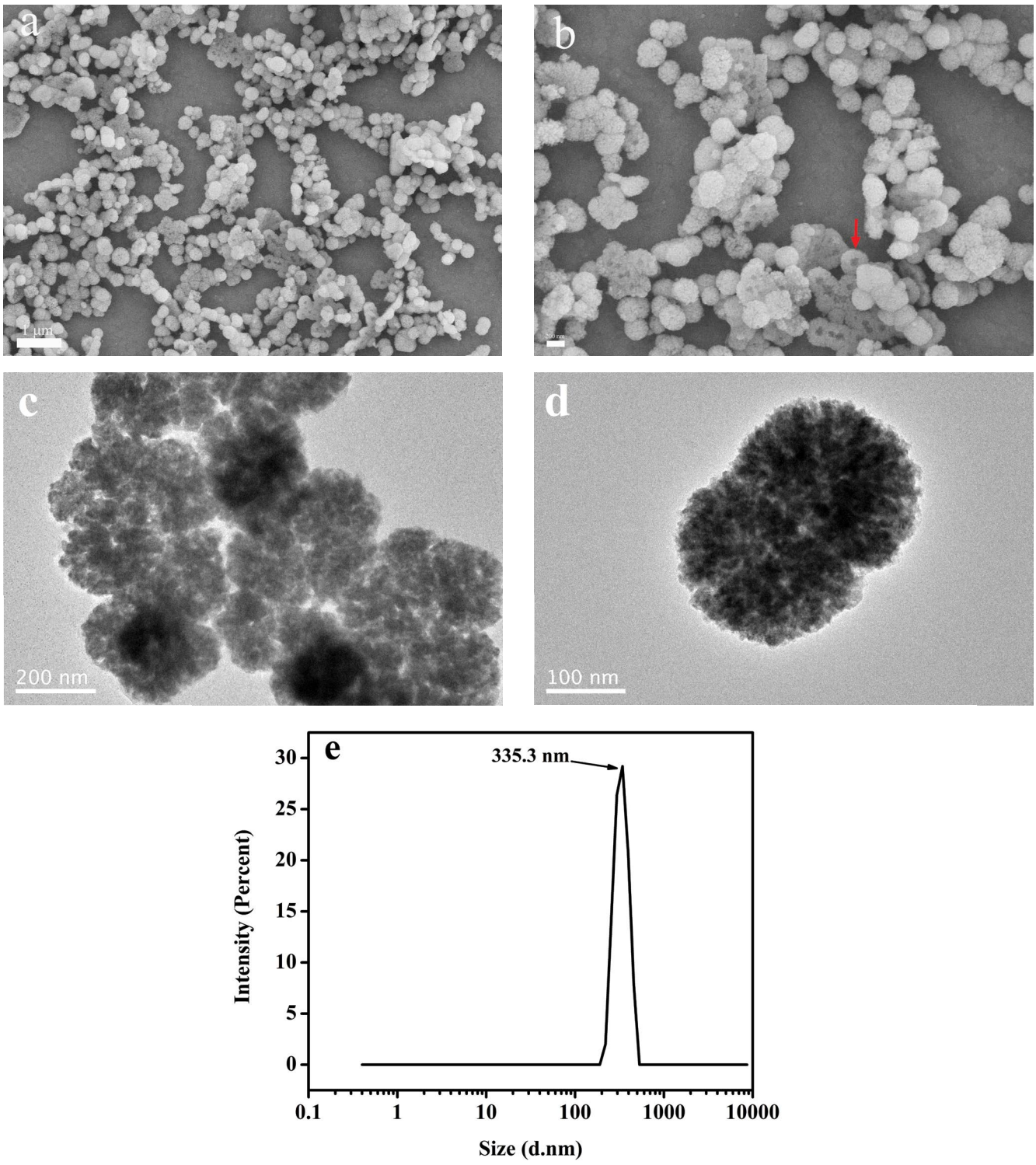

Fig. 2. SEM (a,b), TEM (c,d) images and size distribution (e) of Cu_2O SPs.

steps of adsorption process occur [37,38]. The first linear region represents the transport of MO molecules from bulk solution onto the surface of Cu_2O SPs and the diffusion rate of this stage is the fastest due to the high initial MO concentration gradient. The second linear region is a gradual adsorption stage and corresponds to intraparticle diffusion, which is a rate-controlled stage. The last linear region shows the equilibrium phase, at which intraparticle diffusion further slows down until the adsorption equilibrium reaches. The diffusion rate constant in each step decreases

in the following order: $k_1 > k_2 > k_3$ (Table 2). These results suggested that MO molecules slowly diffused through slit-like pores formed by assembled nanoparticles into Cu_2O SPs.

3.2.2. Adsorption isotherms

Adsorption isotherms clearly describe the relationship between the concentration of dye in solution and the amount of dye adsorbed on the solid phase when both phases are in equilibrium. Langmuir and Freundlich isotherm models were used to analyze the experimental data. The linear forms of Langmuir and Freundlich equations are expressed as follows [39,40]:

$$\text{Langmuir: } \frac{1}{q_e} + \frac{1}{q_{\max}} + \frac{1}{K_L \cdot q_{\max} \cdot C_e} \tag{7}$$

$$\text{Freundlich: } \ln q_e = \ln K_F + \frac{1}{n} \ln C_e \tag{8}$$

where C_e (mg/L) and q_e (mg/g) are the equilibrium concentration of MO in solution and adsorption capacity at equilibrium, respectively. $q_{\max}$ (mg/g) is the theoretical maximum adsorption capacity. K_L (L/mg) and K_F [(mg/g)(L/mg)$^{1/n}$] are the Langmuir constant and the Freundlich constant, respectively. And $1/n$ is the adsorption intensity.

Fig. 7 shows the linear fitting of Langmuir and Freundlich isotherm models and the corresponding parameters are listed in Table 2. According to Fig. 7, the Langmuir model fits the experimental data better than the Freundlich model according to the correlation coefficient (R^2), which indicates MO monolayer coverage on the Cu_2O SPs [33]. The maximum adsorption capacity calculated from the Langmuir equation was 885.0 mg/g (Table 3), which was much higher than other previously reported adsorbents (Table 4).

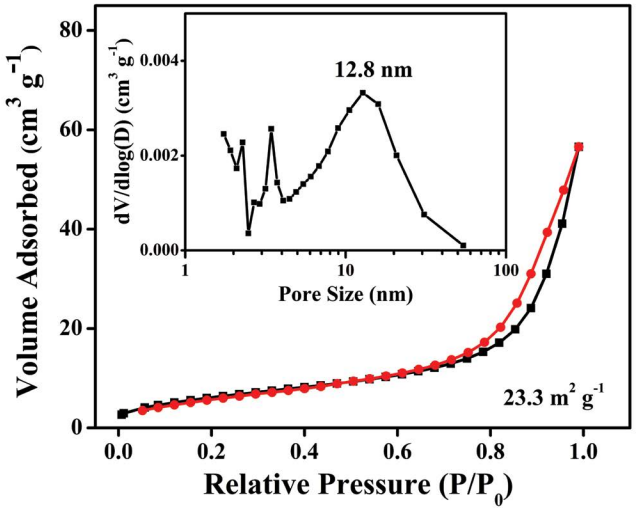

Fig. 3. N_2 adsorption–desorption isotherm of Cu_2O SPs and the corresponding pore-size distribution (inset).

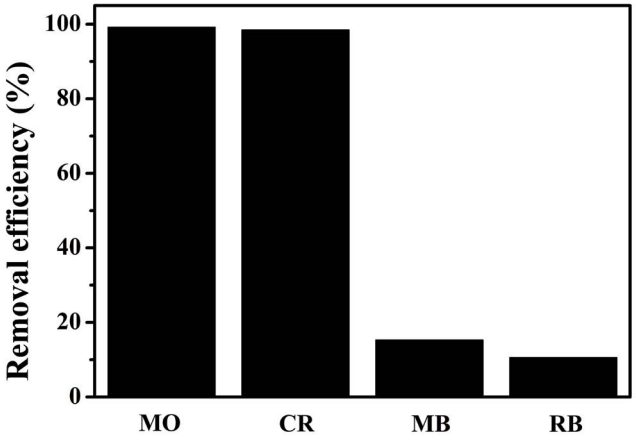

Fig. 4. Adsorption performance of Cu_2O SPs for different cationic and anionic dyes.

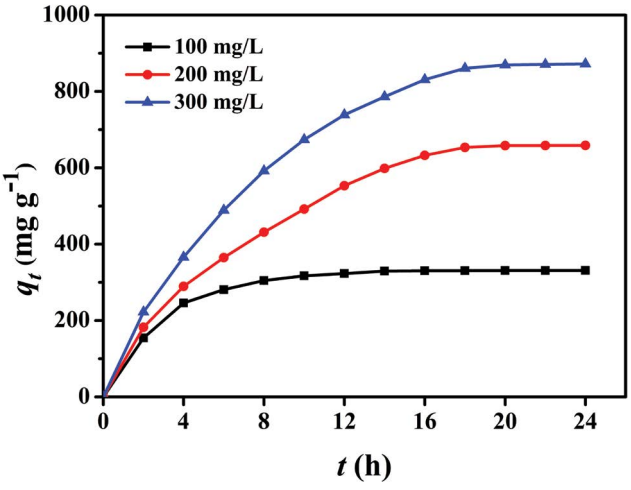

Fig. 5. Effect of contact time and initial dye concentration on the adsorption capacity of MO onto Cu_2O SPs.

Table 1
Pseudo-first-order and pseudo-second-order kinetics model parameters of the Cu_2O SPs

C_0 (mg/L)	$q_{e,exp}$ (mg/g)	Pseudo-first-order			Pseudo-second-order		
		$q_{e,cal}$ (mg/g)	k_1 (h^{-1})	R^2	$q_{e,cal}$ (mg/g)	k_2 (g/mg h)	R^2
100	331.1	189.6	0.220	0.926	333.3	1.01×10^{-5}	0.999
200	659.2	901.0	0.172	0.932	657.5	2.31×10^{-6}	0.999
300	872.3	1,122.5	0.136	0.951	877.2	1.30×10^{-6}	0.999

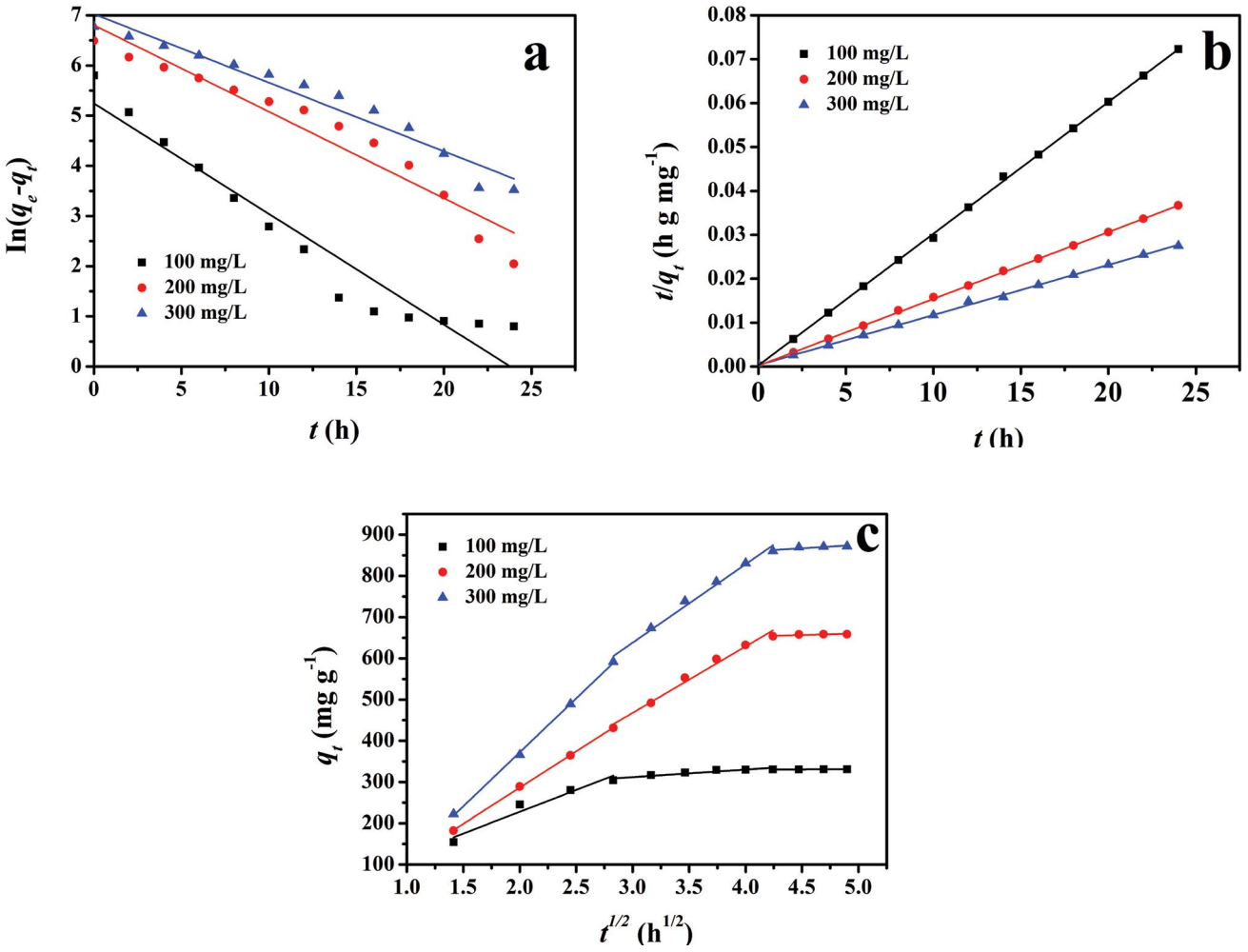

Fig. 6. Pseudo-first-order (a), pseudo-second-order (b), and intraparticle diffusion (c) kinetics for the adsorption of MO on the Cu_2O SPs.

Table 2
Intraparticle diffusion model parameters of the Cu_2O SPs

C_0 (mg/L)	k_1 (mg/g h$^{1/2}$)	c_1 (mg/g)	R^2	k_2 (mg/g h$^{1/2}$)	c_2 (mg/g)	R^2	k_3 (mg/g h$^{1/2}$)	c_3 (mg/g)	R^2
100	105.74	16.62	1	18.28	257.19	0.999	0.59	328.19	0.999
200	175.59	–64.54	1	160.96	–14.88	0.999	7.45	623.18	0.999
300	261.83	–151.57	1	189.96	68.30	0.999	16.55	792.48	0.999

Table 3
Adsorption isotherm parameters of Cu_2O SPs

Langmuir			Freundlich		
K_L (L/mg)	q_{max} (mg/g)	R^2	K_F (mg/g)(L/mg)	1/n	R^2
0.0632	885.0	0.999	136.0	0.408	0.965

3.2.3. *Reusability of Cu_2O SPs*

The reusability of the adsorbent is very important for its practical application. Because Cu_2O is a *p*-type semiconductor with high photoactivity [49], the regeneration of Cu_2O SPs can realize by visible light irradiation. After MO adsorption, the Cu_2O SPs were collected by

Table 4
Comparison of the maximum capacity of MO on various adsorbents

Type of adsorbent	q_{max} (mg/g)	Reference
Cu_2O SPs	885.0	Present work
Graphene-like porous carbon nanostructure	418	[41]
Graphene oxide aerogel	55.6	[42]
Hollow carbon spheres/graphene hybrid aerogels	344.1	[43]
Functionalized carbon nanotubes	310.2	[44]
3D hierarchical graphene oxide-NiFe layered double hydroxide	438	[45]
Fe_3O_4 nanoparticles functionalized activated carbon	150.4	[46]
Polyamidoamine dendrimer gel	680.2	[47]
Cu_2O hollow submicrospheres	446.4	[23]
Copper oxide-poly(m-phenylenediamine) microflowers	264.6	[48]

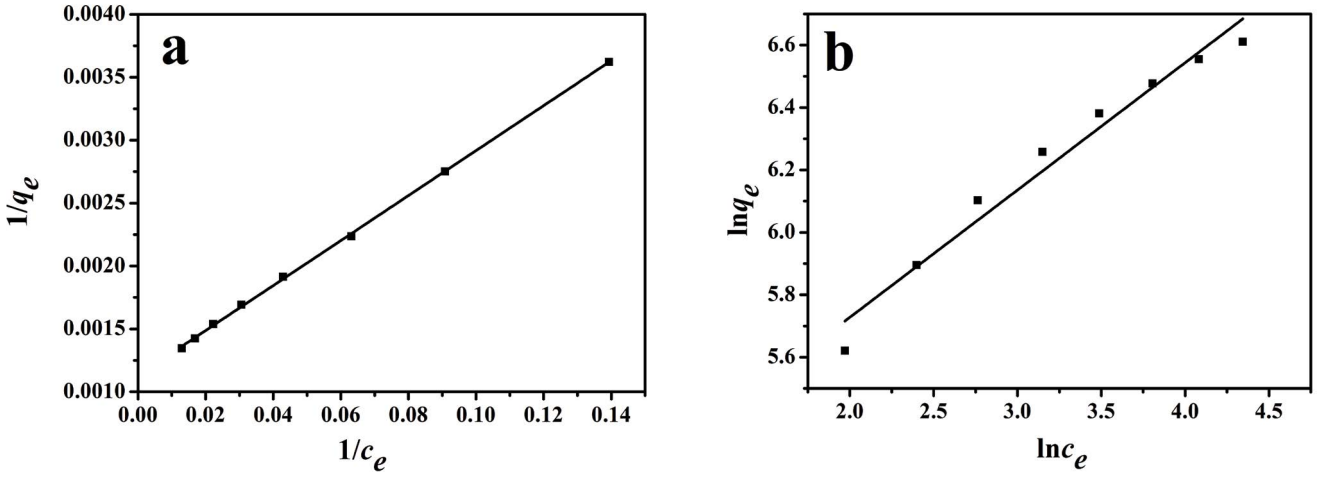

Fig. 7. Langmuir (a) and Freundlich (b) isotherms for MO adsorption on the Cu_2O SPs.

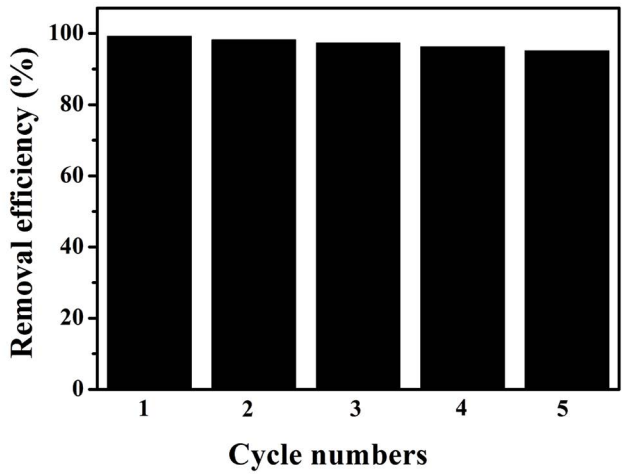

Fig. 8. Cyclability of Cu_2O SPs for MO.

centrifugation and re-dispersed in 50 mL deionized water. The solution was irradiation by visible light at room temperature until the solution was colorless. Then Cu_2O SPs were collected by centrifugation, dried at 60°C for 12 h and reused in the next cycle of adsorption. As shown in Fig. 8, the removal efficiency of MO was no significant reduction after five cycles, which suggested the Cu_2O SPs can be photocatalytically regenerated.

4. Conclusion

In this work, Cu_2O SPs with spherical-like structure were prepared by ultrasound-assisted polyol process using DEG as solvent. The adsorption experiments showed that the prepared Cu_2O SPs had high adsorption capacity toward anionic dyes in aqueous solutions. MO was selected as representational anionic dye to measure the adsorption kinetics and isotherms. The results showed that the adsorption kinetics fitted well with pseudo-second-order model. And the equilibrium data could be well described by the Langmuir isotherm model, with maximum adsorption capacity of 885.0 mg/g. Moreover, Cu_2O SPs can be easily recycled and regenerated by visible light irradiation. Hence, the prepared Cu_2O SPs can be used as a potential adsorbent for the adsorption removal of anionic dyes from wastewater.

Acknowledgements

This work was supported by the National Natural Science Foundation of China (21775013) and Research Program for the Transformation of Scientific and Technological achievements of Huaian City (HA202114).

References

[1] Z.C. Liu, T.A. Khan, M.A. Islam, U. Tabrez, A review on the treatment of dyes in printing and dyeing wastewater by plant biomass carbon, Bioresour. Technol., 354 (2022) 127168, doi: 10.1016/j.biortech.2022.127168.
[2] P. Pattnaik, G.S. Dangayach, A.K. Bhardwaj, A review on the sustainability of textile industries wastewater with and without treatment methodologies, Rev. Environ. Health, 33 (2018) 163–203.
[3] H. Chen, S. Wageh, A.A. Al-Ghamdi, H.Y. Wang, J.G. Yu, C.J. Jiang, Hierarchical C/NiO-ZnO nanocomposite fibers with enhanced adsorption capacity for Congo red, J. Colloid Interface Sci., 537 (2019) 736–745.
[4] H.M. Zhang, Y. Ruan, Y. Feng, M.H. Su, Z.H. Diao, D.Y. Chen, L.A. Hou, P.-H. Lee, K. Shih, L.J. Kong, Solvent-free hydrothermal synthesis of gamma-aluminum oxide nanoparticles with selective adsorption of Congo red, J. Colloid Interface Sci., 536 (2019) 180–188.
[5] G.A. Ismail, H. Sakai, Review on effect of different type of dyes on advanced oxidation processes (AOPs) for textile color removal, Chemosphere, 291 (2022) 132906, doi: 10.1016/j.chemosphere.2021.132906.
[6] Q. Xu, Y.Y. Xu, J.M. Xue, F.H. Zhu, Z.P. Zhong, R.J. Liu, An innovative alcohol-solution combustion-calcination process for the fabrication of $NiFe_2O_4$ nanorods and their adsorption characteristics of methyl blue in aqueous solution, Mater. Res. Express, 8 (2021) 095003.
[7] J. Labanda, J. Sabaté, J. Llorens, Modeling of the dynamic adsorption of an anionic dye through ion-exchange membrane adsorber, J. Membr. Sci., 340 (2009) 234–240.
[8] K. Mustafa, S. Musaddiq, S. Farrukh, S. Ahmad, H. Rasheed, I. Fayyaz, 3-(Aminopropyl)triethoxysilane modified CuO nanoparticles-mediated adsorbent for removal of methylene blue through polymer inclusion membranes transport: optimization of operational variables, Desal. Water Treat., 242 (2021) 274–282.
[9] H.L. Liu, R.X. Sun, S.Y. Feng, D.X. Wang, H.Z. Liu, Rapid synthesis of a silsesquioxane-based disulfide-linked polymer for selective removal of cationic dyes from aqueous solutions, Chem. Eng. J., 359 (2019) 436–445.
[10] J.W. Cui, G.H. Wang, C. Wang, P. Ke, Q. Tian, Y.S. Tian, Characterization, adsorption isotherm, and kinetic of mesoporous silica microspheres for dyeing wastewater, Desal. Water Treat., 217 (2021) 358–366.
[11] J. Tian, J.F. Wei, H. Zhang, Z.Y. Kong, Y.W. Zhu, Z. Qin, Graphene oxide-functionalized dual-scale channels architecture for high-throughput removal of organic pollutants from water, Chem. Eng. J., 359 (2019) 852–862.
[12] A. Naghizadeh, M. Kamranifar, A.R. Yari, M.J. Mohammadi, Equilibrium and kinetics study of reactive dyes removal from aqueous solutions by bentonite nanoparticles, Desal. Water Treat., 97 (2017) 329–337.
[13] Y. Li, T.C. Wang, S.S. Zhang, Y.L. Zhang, L.L. Yu, R.J. Liu, Adsorption and electrochemical behavior investigation of methyl blue onto magnetic nickel-magnesium ferrites prepared via the rapid combustion process, J. Alloys Compd., 885 (2021) 160969, doi: 10.1016/j.jallcom.2021.160969.
[14] Y. Li, S. Pan, Q.M. Yu, X. Ding, R.J. Liu, Adsorption mechanism and electrochemical performance of methyl blue onto magnetic $Ni_{(1-x-y)}Co_yZn_xFe_2O_4$ nanoparticles prepared via the rapid-combustion process, Ceram. Int., 46 (2020) 3614–3622.
[15] R.T. Yin, S.S. Zhang, Y.Y. Xu, J.M. Xue, J.Q. Bi, R.J. Liu, Adsorption mechanism and electrochemical properties of methyl blue onto magnetic $Co_xCu_{(1-x)}Fe_2O_4$ nanoparticles prepared via an alcohol solution of nitrate combustion and calcination process, J. Inorg. Organomet. Polym. Mater., 31 (2021) 3584–3594.
[16] L.L. Yu, Y. Li, S. Pan, W. Huang, R.J. Liu, Adsorption mechanisms and electrochemical properties of methyl blue onto magnetic $Ni_xMg_yZn_{(1-x-y)}Fe_2O_4$ nanoparticles fabricated via the ethanol-assisted combustion process, Water Air Soil Pollut., 231 (2020) 316, doi: 10.1007/s11270-020-04686-9.
[17] J.-M. Yang, Functionally modified metal–organic frameworks for the removal of toxic dyes from wastewater, CrystEngComm., 24 (2022) 434, doi: 10.1039/D1CE01385H.
[18] Z.J. Yang, G.F. Wu, Q.R. Li, H.X. Ai, X.D. Yao, H.B. Ji, Removal of various pollutants from wastewaters using an efficient and degradable hypercrosslinked polymer, Sep. Sci. Technol., 56 (2020) 860–869.
[19] D.W. Lan, H.W. Zhu, J.W. Zhang, S. Li, Q.H. Chen, C.X. Wang, T. Wu, M.X. Xu, Adsorptive removal of organic dyes via porous materials for wastewater treatment in recent decades: a review on species, mechanisms and perspectives, Chemosphere, 293 (2022) 133464, doi: 10.1016/j.chemosphere.2021.133464.
[20] Y. Cheng, T. Cao, Z.G. Xiao, H.J. Zhu, M. Yu, Photocatalytic treatment of methyl orange dye wastewater by porous floating ceramsite loaded with cuprous oxide, Coatings, 12 (2022) 286, doi: 10.3390/coatings12020286.
[21] M. Singh, D. Jampaiah, A.E. Kandjani, Y.M. Sabri, E. Della Gaspera, P. Reineck, M. Judd, J. Langley, N. Cox, J. van Embden, E.L.H. Mayes, B.C. Gibson, Oxygen-deficient photostable Cu_2O for enhanced visible light photocatalytic activity, Nanoscale, 13 (2018) 6039–6050.
[22] X. Zhang, Y. Zhang, D. Wang, F.Y. Qu, Investigation of adsorption behavior of Cu_2O submicro-octahedra towards Congo red, J. Nanomater., 2014 (2014) 619239, doi: 10.1155/2014/619239.
[23] X.Q. Ge, H.M. Hu, C.H. Deng, Q. Zheng, M. Wang, G.Y. Chen, Facile sonochemical synthesis of hierarchical Cu_2O hollow submicrospheres with high adsorption capacity for methyl orange, Mater. Lett., 141 (2015) 214–216.
[24] L. Huang, F. Peng, H. Yu, H.J. Wang, Synthesis of Cu_2O nanoboxes, nanocubes and nanospheres by polyol process and their adsorption characteristic, Mater. Res. Bull., 43 (2008) 3047–3053.
[25] C. Xu, X. Wang, L.C. Yang, Y.P. Wu, Fabrication of a graphene-cuprous oxide composite, J. Solid State Chem., 182 (2009) 2486–2490.
[26] H. Dong, Y.C. Chen, C. Feldmann, Polyol synthesis of nanoparticles: status and options regarding metals, oxides, chalcogenides, and non-metal elements, Green Chem., 17 (2015) 4107–4132.
[27] H. Enamul, M.K. Chang, H.J. Sung, Facile synthesis of cuprous oxide using ultrasound, microwave and electric heating: effect of heating methods on synthesis kinetics, morphology and yield, CrystEngComm, 12 (2011) 4060–4068.
[28] Y.Y. Xiao, X.L. Tong, Y.F. Zhang, X.D. Han, Y.Y. Wang, G.Q. Jin, Y. Qin, X.Y. Guo, Cuprous oxide nanoparticles dispersed on reduced graphene oxide as an efficient electrocatalyst for oxygen reduction reaction, Chem. Commun., 48 (2012) 1892–1894.
[29] L.F. Zhong, A.D. Tang, P. Yan, J.J. Wang, Q.J. Wang, X. Wen, Y. Cui, Palygorskite-template amorphous carbon nanotubes as a superior adsorbent for removal of dyes from aqueous solutions, J. Colloid Interface Sci., 537 (2019) 450–457.
[30] J. Ye, L.N. Jin, X.S. Zhao, X.Y. Qian, M.D. Dong, Superior adsorption performance of metal-organic-frameworks derived magnetic cobalt-embedded carbon microrods for triphenylmethane dyes, J. Colloid Interface Sci., 536 (2019) 483–492.
[31] Y. Yu, L.L. Ma, W.Y. Huang, J.L. Li, P.K. Wong, J.C. Yu, Coating MWNTs with Cu_2O of different morphology by a polyol process, J. Solid State Chem., 178 (2005) 1488–1494.
[32] Z.C. Orel, A. Anzlovar, G. Drazic, M. Zigon, Cuprous oxide nanowires prepared by an additive-free polyol process, Cryst. Growth Des., 7 (2007) 453–458.
[33] C.S. Lei, M. Pi, D.F. Xu, C.J. Jiang, B. Cheng, Fabrication of hierarchical porous ZnO-Al_2O_3 microspheres with enhanced adsorption performance, Appl. Surf. Sci., 426 (2017) 360–368.

[34] J.X. Shu, Z.H. Wang, Y.J. Huang, N. Huang, C.G. Ren, W. Zhang, Adsorption removal of Congo red from aqueous solution by polyhedral Cu_2O nanoparticles: kinetics, isotherms, thermodynamics and mechanism analysis, J. Alloys Compd., 633 (2015) 338–346.
[35] C. Wang, Y. Le, B. Cheng, Fabrication of porous ZrO_2 hollow sphere and its adsorption performance to Congo red in water, Ceram. Int., 40 (2014) 10847–10856.
[36] V. Srivastava, Y.C. Sharma, M. Sillanpää, Application of nano-magnesso ferrite (*n*-$MgFe_2O_4$) for the removal of Co^{2+} ions from synthetic wastewater: kinetic, equilibrium and thermodynamic studies, Appl. Surf. Sci., 338 (2015) 42–54.
[37] C.L. Qi, L.H. Xu, M.X. Zhang, M. Zhang, Fabrication and application of hierarchical porous carbon for the adsorption of bulky dyes, Microporous Mesoporous Mater., 290 (2019) 109651, doi: 10.1016/j.micromeso.2019.109651.
[38] C.S. Lei, M. Pi, B. Cheng, C.J. Jiang, J.Q. Qin, Fabrication of hierarchical porous ZnO/NiO hollow microspheres for adsorptive removal of Congo red, Appl. Surf. Sci., 435 (2018) 1002–1010.
[39] I. Langmuir, The adsorption of gases on plane surfaces of glass, mica and platinum, J. Am. Chem. Soc., 40 (1918) 1361–1403.
[40] H. Freundlich, Over the adsorption in solution, J. Phys. Chem., 57 (1906) 1100–1107.
[41] K. Gupta, D. Gupta, O.P. Khatri, Graphene-like porous carbon nanostructure from Bengal gram bean husk and its application for fast and efficient adsorption of organic dyes, Appl. Surf. Sci., 476 (2019) 647–657.
[42] T.H. Tu, P.T.N. Cam, L.V.T. Huy, M.T. Phong, H.M. Nam, N.H. Hieu, Synthesis and application of graphene oxide aerogel as an adsorbent for removal of dyes from water, Mater. Lett., 238 (2019) 134–137.
[43] P.C. Hou, G.J. Xing, L.Y. Tian, G. Zhang, H. Wang, C.N. Yu, Y.L. Li, Z.L. Wu, Hollow carbon spheres/graphene hybrid aerogels as high-performance adsorbents for organic pollution, Sep. Purif. Technol., 213 (2019) 524–532.
[44] R.K. Ibrahim, A. El-Shafie, L.S. Hin, N.S.B. Mohd, M.M. Aljumaily, S. Ibraim, M.A. AlSaadi, A clean approach for functionalized carbon nanotubes by deep eutectic solvents and their performance in the adsorption of methyl orange from aqueous solution, J. Environ. Manage., 235 (2019) 521–534.
[45] Y.Q. Zheng, B. Cheng, W. You, J.Y. Yu, W.K. Ho, 3D hierarchical graphene oxide-NiFe LDH composite with enhanced adsorption affinity to congo red, methyl orange and Cr(VI) ions, J. Hazard. Mater., 369 (2019) 214–225.
[46] X.D. Liu, J.F. Tian, Y.Y. Li, N.F. Sun, S. Mi, Y. Xie, Z.Y. Chen, Enhanced dyes adsorption from wastewater via Fe_3O_4 nanoparticles functionalized activated carbon, J. Hazard. Mater., 373 (2019) 397–407.
[47] Y.X. Duan, Y.H. Song, L. Zhou, Facile synthesis of poly-amidoamine dendrimer gel with multiple amine groups as a super adsorbent for highly efficient and selective removal of anionic dyes, J. Colloid Interface Sci., 546 (2019) 351–360.
[48] T.T. Guo, X.Y. Kang, T.T. Zhang, F. Liao, Uniform copper oxide-poly(m-phenylenediamine) microflowers: synthesis and application for the adsorption of methyl orange, RSC Adv., 5 (2015) 17817–17823.
[49] S. Rasheed, Z. Batool, A. Intisar, S. Riaz, M. Shaheen, R. Kousar, Enhanced photodegradation activity of cuprous oxide nanoparticles towards Congo red for water purification, Desal. Water Treat., 227 (2021) 330–337.